



Ni-Zn/CeO₂ nanocomposites for enhanced adsorptive removal of 4-chlorophenol

Nitish Semwal¹ · Divya Mahar¹ · Manjunath Chatti³ · Rajesh Kumar² · Mahesh Chandra Arya¹

Received: 26 March 2024 / Accepted: 5 August 2024 / Published online: 12 August 2024
© The Author(s), under exclusive licence to Springer-Verlag GmbH Germany, part of Springer Nature 2024

Abstract

Chlorophenols are one of the major organic pollutants responsible for the contamination of water bodies. This study explores the application of Ni-Zn/CeO₂ nanocomposites, synthesized via the aqueous co-precipitation method, as effective adsorbents for the 4-chlorophenol removal from aqueous solutions. The nanocomposites' chemical and structural characteristics were assessed using different physical characterization methods, viz. X-ray diffraction, transmission electron microscopy, Fourier transform infrared spectroscopy, zeta potential, using a Box-Behnken design within response surface methodology, optimal conditions of pH 3, temperature 20 °C, contact time 120 min, adsorbent dosage 0.05 g, and 4-chlorophenol concentration 50 ppm are identified. Among the nanocomposites tested, NZC 20:10:70, with 20% Ni and 10% Zn, achieves enhanced performance, removing 99.1% of 4-chlorophenol within 2 h. Adsorption kinetics follow the pseudo-second-order model and equilibrium data fit the Freundlich isotherm. Thermodynamic analysis indicates an exothermic and spontaneous process. The adsorption capacity of NZC 20:10:70 shows significant enhancement, growing from 19.85 mg/g at 10 ppm to 96.33 mg/g at 50 ppm initial concentration. Physical characterization confirms NZC 20:10:70's superior properties, including a high surface area of 118.471 m²/g. Evaluating economic viability, NZC 20:10:70 demonstrates robust reusability, retaining 85% efficiency over eight regeneration cycles. These results highlight NZC 20:10:70 as a promising adsorbent for effective and sustainable chlorophenol removal in water treatment.

Keywords Adsorption · Ni-Zn/CeO₂ · Nanocomposite · Response surface methodology · Freundlich · 4-Chlorophenol

Introduction

The rapid surge in environmental pollution can be primarily attributed to the process of industrialization (Lu et al. 2019). It has resulted in increased production and use of toxic chemicals leading to ecological imbalance. The phenols, especially chlorophenols, used in insecticides, augment the severity of the problem by their toxicity (Mishra et al. 2023; Azizi et al. 2021). The organic pollutants present in

industrial wastewater are difficult to remove by conventional treatment.

Chlorophenols, classified as endocrine-disrupting compounds in the phenolic category, are highly toxic and have carcinogenic effects (Hamidon et al. 2022). Phenolic pollutants are contaminating the environment, raising a threat to human as well as ecosystem health (Ki et al. 2017). Studies have indicated that prolonged consumption of water contaminated with chlorophenols can lead to serious health issues, including but not limited to anaemia and dizziness (Allaboun and Al-Rub 2016). Furthermore, it has the potential to impact critical bodily systems, such as the central nervous system and the liver (Varsha et al. 2022).

Chlorophenols are widely used in various industries, serving as essential components in the production of pharmaceuticals, dyes, lubricants, preservatives, pesticides, fungicides, and herbicides (Yadav et al. 2023). The chlorophenols can enter water bodies from various sources, such as industrial waste, pesticide use, and from disintegration of chlorinated hydrocarbons (Zhao et al. 2022). Chlorophenols

Responsible Editor: Tito Roberto Cadaval Jr

✉ Mahesh Chandra Arya
mcarya181@gmail.com

¹ Department of Chemistry, DSB Campus, Kumaun University, Nainital, Uttarakhand 263002, India

² Department of Chemistry, SSJ Campus, SSJ University, Almora, Uttarakhand, India

³ Nanochemistry, Istituto Italiano di Tecnologia, Via Morego 30, 16163 Genova, Italy

are a consequential byproduct of the chlorination process, which is commonly utilized to treat wastewater for sanitation purposes. However, the unintended formation of these by-products causes contamination of soil, groundwater, and surface water (Lu et al. 2019). 4-Chlorophenol is the most toxic of the mono-chlorophenols and can be easily absorbed by humans. Its widespread presence in wastewater and high toxicity makes it urgent to develop methods for its removal from aqueous solutions (Gao et al. 2021).

Different approaches employed for the 4-chlorophenol removal from its aqueous solution include removal through membrane separation (Goel et al. 2010), biological degradation (Gómez et al. 2012), solvent extraction [Adeyemi et al. 2020], and adsorption, catalytic oxidation (Wang et al. 2022). However, these methods have their own limitations. Adsorption stands out as the appropriate method for pollutant removal due to its simplicity in operation, exceptional effectiveness, cost-effectiveness, and the wide array of available adsorbents [Rahman and Ahmad 2023].

Recent advancements in environmental remediation have highlighted the effectiveness of various nanocomposite materials for treating wastewater contaminated with phenolic compounds and their derivatives. These include the use of sulphur-doped activated carbon for catalytic oxidation of phenolic compounds (Guo et al. 2017), ZrO₂/LDH under UV light for photocatalytic removal of phenols (Melchor-Lagar et al. 2020), layered double hydroxides/single-walled carbon nanotubes for both phenol and 4-chlorophenol (Zhang et al. 2019), magnetic Fe₃O₄/activated carbon for combined adsorption and Fenton oxidation of phenolic compounds (Duan et al. 2020), porous and ultrafine nitrogen-doped carbon nanofibers from bacterial cellulose [Gao et al. 2021], and even biodegradation methods using isolated *Bacillus subtilis* for chlorophenol removal [Patel et al. 2022]. Bayramoglu and Arica (2023) demonstrated the use of *Lentinus sajor-caju* immobilized in stable Calcium alginate beads for efficient phenol and derivative degradation. Further advancements include Doyo et al.'s (2023) Polyaniline@Waste Cellulosic nanocomposites for phenol decontamination and Jagaba et al.'s (2023) biochar-based geopolymer nanocomposites, demonstrating phenol removal efficiencies of 61.94% and 74.44% for BEAS and GEAS bioreactors, respectively. Kumar et al. (2023) developed a cellulose/graphene-oxide composite, capable of removing 86% of phenol within 40 min, highlighting its rapid and efficient wastewater treatment potential. Several nanomaterials have further been investigated for their adsorptive efficiency towards a variety of phenolic and other organic pollutants including graphene oxide-bentonite nanocomposites (Ayoob et al. 2024), GO/bentonite/MgFeAl-LTH nanocomposite (Bahadi et al. 2024), bio-derived carbon-based nanocomposites (DP-IO) (Ajmi et al. 2024), and montmorillonite-Fe₃O₄-humic acid (MFH) nanocomposites (Rodrigues et al.

2024). The recent literature review reveals that the mixed-metal oxide nanocomposite involving rare earth metals has been under-explored for their adsorption efficiency towards 4-chlorophenol and other organic pollutants.

Previous studies have predominantly explored catalytic oxidation, photocatalytic degradation, biodegradation, and combined adsorption with oxidation processes using materials like activated carbon, metal oxides, and biocatalysts for removing 4-chlorophenol (4-CP) from aqueous solutions, with limited focus on adsorption studies. In this study, we explore and develop mixed-metal oxide nanocomposites containing rare earth metals for the efficient adsorption of 4-chlorophenol. Unlike conventional approaches using organic or graphene-based materials, this study focuses on leveraging the unique properties of rare earth metals within nanocomposites. The adsorption efficiency of Ni-Zn/CeO₂ nanomaterials (with three different compositions) has been investigated for the removal of 4-chlorophenol. The effects of optimization factors like pH, time, temperature, quantity of adsorbent dose, and concentration of 4-chlorophenol on the adsorption process were investigated using response surface methodology (RSM) and a Box-Behnken design (BBD). Also, the kinetic as well as thermodynamic studies of the adsorption process have been undertaken to deduce the influence of experimental parameters on the adsorption ability of the nanocomposites.

Experimental

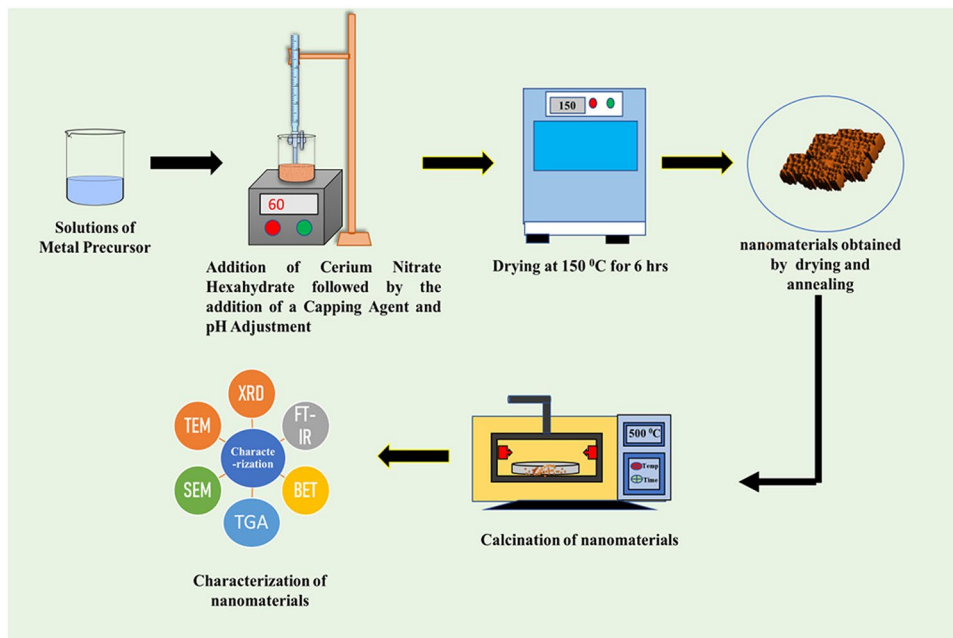
Materials

Nickel sulphate (NiSO₄) (99% purity), cerium nitrate hexahydrate (Ce(NO₃)₃·6H₂O) 99%, zinc sulphate (ZnSO₄) 99%, 4-chlorophenol (Cl-C₆H₄OH) 99.9%, and cetyltrimethylammonium bromide (CTAB) 99% were of analytical grade and acquired from Sigma-Aldrich and were used as obtained. Throughout the study, deionized water was used for all purposes.

Synthesis route of Ni-Zn/CeO₂ nanocomposites

Three distinct compositions of Ni-Zn/CeO₂ nanocomposites were synthesized by the aqueous coprecipitation method (Semwal et al. 2023). According to the weight percentage of Ni, Zn, and Ce precursors, these three compositions have been named NZC 10:20:70 (means precursors of Ni/Zn/Ce are in the ratio of 10:20:70), NZC 15:15:70, and NZC 20:10:70. The schematic synthesis of Ni-Zn/CeO₂ nanocomposites is illustrated in Fig. 1 The aqueous solutions of NiSO₄ and ZnSO₄ with a specific amount for each nanocomposite are prepared separately. Then, 100 mL of each of these solutions were then mixed to create a unified metal

Fig. 1 Diagrammatic representation of the synthesis process of Ni-Zn/CeO₂ nanocomposites



precursor solution. While maintaining a temperature of 60 °C and stirring at 500 rpm, a cerium nitrate hexahydrate (70 wt%, 100 ml) solution was dropwise added and stirred for 30 min. This ensured thorough mixing and reaction between the cerium nitrate and Ni and Zn metal precursors. Subsequently, a solution of the CTAB (3.46 gm in 100 ml), which acts as a capping agent, was introduced drop by drop. Thereafter, the resultant mixture pH was brought to 10 by the addition of 1 M NaOH. After completing the reaction, the precipitate was collected through filtration, and extensive washing with deionized water was performed to remove unreacted metal precursors and other contaminants. The removal was ensured by testing the ions in the filtrate. The further process involved repeated washes with ethanol. The washed precipitate was then dried for 2 h at 80 °C in an oven. Subsequently, the dried material was further annealed in a high-temperature tube furnace at 400 °C for 4 h with a ramping rate of 5 °C min⁻¹ to enhance its crystallinity and eliminate any remaining organic components. Finally, the material was finely grounded and stored for further use.

Characterization

The determination of crystal structure was facilitated by X-ray diffraction (XRD), which was carried out with a Bruker D8-Advance P-X-ray diffractometer that was operated at 40 mA and 30 kV utilizing Cu-K α radiation. Crystal structure determination involved collecting diffraction data throughout a 2 θ range of 10°–90°.

Gas sorption analysis was determined by the Quantachrome® ASiQwin™-Automated Gas Sorption instrument, which provides valuable insights into the surface area and size

of pores. Fourier transform infrared (FT-IR) analysis, was performed using the PerkinElmer Spectrum instrument. Scanning electron microscopy (SEM) with the Carl Zeiss Model Supra 55 instrument allowed for the visualization of surface morphology at high resolution. The thermogravimetric analysis (TGA) was performed using PerkinElmer and provided information on the thermal stability of the nanocomposites. Transmission electron microscopy (TEM) was analysed using the JEOL JEM 2100 PLUS which offered detailed images and structural information at the nanoscale. Zeta potential measurement was performed using Anton Paar zeta potential analyser.

Experimental framework

A comprehensive investigation was performed on the impact of four key adsorption parameters on the adsorptive removal of 4-chlorophenol by NZC nanocomposites using a Box-Behnken design (BBD) under response surface methodology (RSM) approach with ANOVA. The result of BBD models involves a graphical analysis. This analysis includes examining the distribution of residuals and comparing the actual removal values with the predicted values for the elimination of 4-chlorophenol using the NZC 20:10:70 nanocomposite (as it shows excellent adsorptive removal among three nanocomposites), whereas analysis of variance (ANOVA) is a statistical technique applied to assess the validity of the applied models for 4-chlorophenol removal and evaluate the significance of the data associated with this removal process. The Stat-Ease Design Expert software was employed to design and analyse adsorption experiments as well as statistically evaluate the data. The levels and coded values of the independent parameters are represented in Table 1.

Table 1 Code, actual variables, and corresponding levels in BBD

Factor	Variable	Low	High
A	pH	2	10
B	Contact time (min)	10	120
C	Adsorbent dose (g/L)	0.01	0.05
D	Temperature (°C)	10	60

To investigate the adsorption isotherm, 0.05 g/L of adsorbent was in contact with 100 mL of 4-chlorophenol solutions at various concentrations at pH 3.0. This contact was maintained for 2 h with constant agitation at room temperature. The contact time study revealed that after 2 h, the equilibrium was reached, and calculating the difference between the two concentration levels yielded the amount of 4 chlorophenol absorbed (in %) on the adsorbent's surface. The efficiency of adsorption depicted as adsorption efficiency of adsorbent towards 4-chlorophenol is determined by applying Eq. 1 (Semwal et al. 2023):

$$\text{adsorption efficiency} = \frac{(C_o - C_e)}{C_o} \times 100 \quad (1)$$

where C_o denotes the initial concentration of the 4-chlorophenol solution (mg/L) and C_e represents the final concentration of 4-chlorophenol in the sampled aliquot (mg/L).

The adsorbent was extracted from the reaction mixture using a standardized leaching procedure. The procedure required multiple washing using organic solvents, deionized water, and sodium hydroxide (NaOH), and then drying for two hours at 100 °C in a hot air oven. To evaluate the adsorbents' recyclability ability subsequent adsorption assays were also undertaken (*vide infra*).

Adsorption isotherm

An isotherm provides insights into the quantity of adsorbent that adheres to the surface per unit mass of the adsorbate at a specific temperature (Lan et al. 2022). Adsorption capacity at equilibrium is expressed by q_e , whereas the concentration of adsorbate in the liquid phase is denoted by C_e . To explain the isotherm curve, three distinct isotherm models were used, namely the Langmuir, Freundlich, and Temkin isotherm models.

The Langmuir model can be presented in linear form by Eq. 2 (Langmuir 1918):

$$\frac{C_e}{q_e} = \frac{1}{q_m K_L} + \frac{C_e}{q_m} \quad (2)$$

$$q_e = \left(\frac{C_o - C_e}{m} \right) * V \quad (3)$$

The symbol C_e represents the 4-chlorophenol concentration at equilibrium (mg/L), q_e (calculated by Eq. 3 (Arica et al. 2022)) stands for the quantity of 4-chlorophenol adsorbed (mg/g), and q_m signifies the adsorption capacity measured in mg/g, whereas the Langmuir constant is denoted as K_L , and it depends on the material's porosity and surface area, C_o represents the initial 4-CP Concentration, V is the volume of the solution (L), and m is the mass of adsorbent in gm.

The Freundlich isotherm is expressed as Eq. 4 (Freundlich and Heller 1939):

$$\log q_e = \log K_F + \frac{1}{n} \log C_e \quad (4)$$

where K_F represents the adsorption capacity (L/mg) and $1/n$ represents the adsorption intensity.

The Temkin isotherm model postulates a linear decrease in adsorption heat for all layers as surface coverage increases, accounting for the influence of indirect interaction of adsorbent-adsorbate (Ayawei et al. 2017).

The Temkin Isotherm is expressed in Eq. 5 (Emmett and Kummer 1943):

$$q_e = \frac{RT}{b_T} \ln A_T + \frac{RT}{b_T} \ln C_e \quad (5)$$

where b_T represents Temkin heat of adsorption constant ($L \cdot mg^{-1}$), R represents gas constant, and A_T represents equilibrium binding constant.

Thermodynamics studies

The thermodynamic parameters such as Gibbs free energy change (ΔG°), entropy change (ΔS°), and enthalpy change (ΔH°), of the process of adsorption of 4-chlorophenol onto Ni-Zn/CeO₂ nanomaterials were also determined by carrying out the thermodynamic studies. The experiments were conducted at temperatures ranging from 10 to 60 °C (283–333 K). and ΔG° is calculated by Eq. 6 (Tran et al. 2021):

$$\Delta G^\circ = -RT \ln K \quad (6)$$

where K_{ads} is equilibrium adsorption constant and it is calculated in Eq. 7:

$$K_{ads} = \frac{q_e}{C_e} \quad (7)$$

where q_e (mg/g) represents the equilibrium adsorption capacity and C_e (mg/g) is the equilibrium concentration of the pollutant in the solution.

ΔH° and ΔS° were calculated by plotting $\ln K_{ads}$ vs $1/T$ and applying Van't Hoff's Eq. 8 (Al-Ghouti and Al-Absi 2020):

$$\ln K_{ads} = \frac{\Delta S^\circ}{R} - \frac{\Delta H^\circ}{T} \left(\frac{1}{T} \right) \quad (8)$$

where ΔS° is the standard entropy change.

Kinetic studies

The kinetics of adsorption gauges the speed at which adsorption of 4-chlorophenol occurs on the Ni-Zn/CeO₂ nanocomposite. In our experiments, the data underwent analysis utilizing both the pseudo-first and pseudo-second order rate equations to examine the adsorption process and ascertain the step controlling the rate. Equation 9 (Lagergren 1898) illustrates the pseudo-first-order model as follows:

$$q_t = q_e (1 - e^{-k_1 t}) \quad (9)$$

Here, q_e signifies the equilibrium capacity measured in milligrams per gram (mg/g), q_t represents the adsorption capacity at time t in mg/g, and K_1 (in min⁻¹) denotes the rate constant for the pseudo-first-order reaction. The pseudo-second-order model is articulated through Eq. 10 (Ho and McKay 1999):

$$q_t = \frac{q_e^2 k_2 t}{1 + q_e k_2 t} \quad (10)$$

where K_2 denotes the pseudo-second-order rate constant.

q_t which represents the adsorption capacity at time t is calculated by Eq. 11 (Arica et al. 2022):

$$q_t = \left(\frac{C_o - C_t}{m} \right) * V \quad (11)$$

where C_o is the initial concentration of the adsorbate in the solution (mg/L), C_t is the concentration of the adsorbate in the solution at time t (mg/L), V is the volume of the solution (L), and m is the mass of the adsorbent (g).

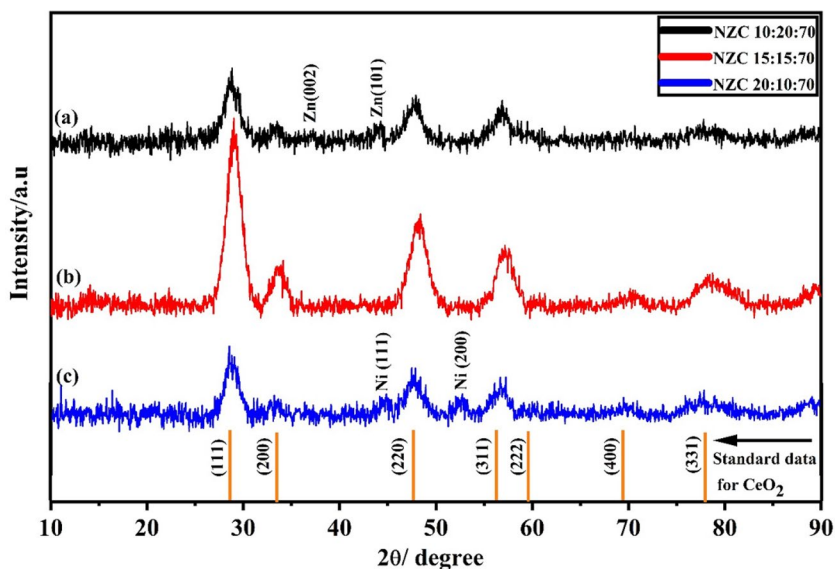
Result and discussion

Powder X-ray diffraction analysis

XRD patterns of the three synthesized nanomaterials are shown in Fig. 2a–c. XRD spectrum of NZC 15:15:70 (Fig. 2b) has only the standard peaks of CeO₂ at 2θ values 28.5, 33.9, 47.8, 56.2, 58.5, and 69.10 corresponding to (111), (200), (220), (311), (222), and (400) lattice planes, respectively (Ramasamy et al. 2018). There are no peaks related to Ni/ NiO or Zn/ZnO. It reveals the formation of a solid solution where Zn and Ni are incorporated in the lattice of CeO₂ preferably by replacing the Ce ions. The shifting of the peaks towards the right to the standard values further supports the doping of Ni and Zn to the CeO₂, leading to the formation of bimetal doped cerium oxide nanoparticles at this composition.

Whereas XRD of NZC 10:20:70 (Fig. 2a) has two characteristic peaks of Zn at 2θ values 36.4° and 43.28° along with the standard peaks of CeO₂ mentioned in the previous paragraph (Qasim et al. 2016), but this material has no peaks for Ni/ NiO, further revealing that Ni ions which are in smaller ratios get incorporated into the CeO₂ lattice. However, the element with a higher ratio (Zn in this case) is expressed as a different phase leading to the formation of a multiphase nanocomposite that has CeO₂ along with Zn. The XRD of NZC 20:10:70 (Fig. 2c) also reveals the same trend. It has Ni elements in higher ratios. The XRD has two characteristic

Fig. 2 XRD characteristics of NZC nanocomposite **a** NZC 10:20:70, **b** NZC 15:15:70, and **c** 20:10:70



peaks of Ni at 44.53° and 52.26° along with the standard peaks of CeO_2 but no peak for Zn (Al-Thabaiti et al. 2019).

Overall, the XRDs confirm that when Ni and Zn are mixed with CeO_2 , there is a threshold ratio until which the elements are incorporated into the lattice of the CeO_2 which is 15:15:70. There is a formation of bimetal doped CeO_2 nanoparticles until this ratio of doping. But once the element crosses this limit, it is no longer incorporated into the lattice and forms a different phase leading to the formation of nanocomposite. Similar facts have been reported in literature where mixing to a certain extent forms doped nanomaterial and mixing beyond this extent leads to the formation of nanocomposites (Saravanan et al. 2013; Wang et al. 2014).

In a nutshell, NZC 15:15:70 is a bimetal doped CeO_2 nanoparticle, whereas NZC 10:20:70 and NZC 20:10:70 is a nanocomposite with two phases.

The Debye-Scherrer formula (Eq. 12 (Basak et al. 2022)) is utilized to determine the crystallite size of the synthesized NZC nanocomposites (NCs):

$$\text{crystallite size } (\phi) = \frac{0.94\lambda}{\beta \cos\theta} \quad (12)$$

where the symbol β denotes the full-width at half-maximum (FWHM) of the X-ray diffraction (XRD) peak with the highest intensity and θ represents the corresponding Bragg diffraction angle. The X-ray source employed had a wavelength

of 0.1504 nm. The shape factor, known as the constant, was established at 0.94. The average crystallite size was found to be 5.09 ± 0.60 nm for NZC 10:20:70, 5.34 ± 0.60 nm for NZC 15:15:70, and 5.28 ± 0.92 nm for NZC 20:10:70. So bimetal-doped nanoparticles have bigger crystallite size than the nanocomposites.

FT-IR analysis

All three nanomaterials were subjected to the FT-IR analysis before the adsorption process and after the adsorption experiments. The FT-IR graphs for each case are given in Fig. 3a–f.

Among the synthesized nanomaterials, NZC 20:10:70 shows the highest adsorptive removal capacity toward 4-chlorophenol. Its FT-IR spectra before adsorption have the Zn–O vibrations at 495.38 and 598.99 cm^{-1} (Murali et al. 2017), C–O stretching (1104.32 cm^{-1}) (Nurfani et al. 2020), O–H deformation (1636.43 cm^{-1}) (Bai et al. 2014), and axial O–H stretching (3243.21 cm^{-1}) (Da Silva et al. 2019), while post-adsorption, new peaks emerge at 1046.09 cm^{-1} (C–OH stretching) (Zhang et al. 2022), 1515.31 cm^{-1} (C=C stretching) (Pancholi et al. 2022), and 3310.80 cm^{-1} (–O–H bond absorption) (Shi et al. 2022), elucidating molecular changes on the catalyst surface. The other two compositions also have different pre- and post-adsorption peaks in IR spectra which have been tabulated in Table 2.

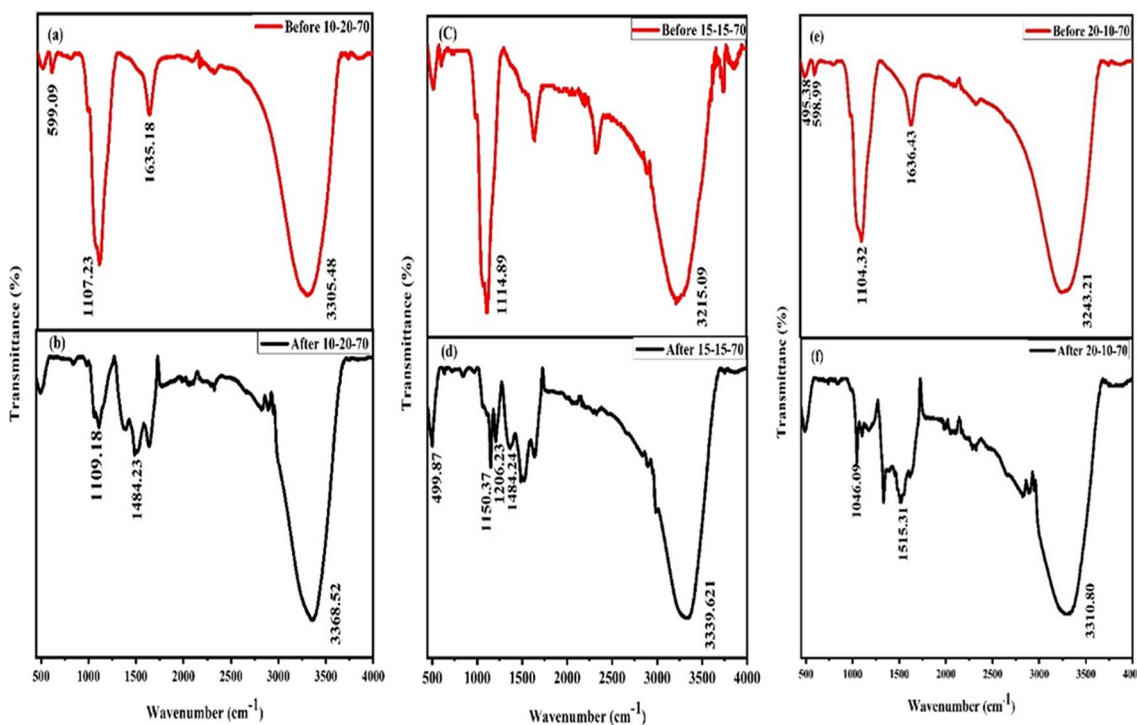


Fig. 3 FT-IR of NZC nanocomposite before and after adsorption (a), (b) NZC 10:20:70 (c), (d) NZC 15:15:70 (e), (f) NZC 20:10:70 (pH = 3, 4-CP concentration = 50 ppm, adsorbent dose = 0.05 g, contact time = 0 min and 120 min, T = 20 °C, volume of solution = 100 ml)

Table 2 FT-IR analysis for Ni-Zn/CeO₂ nanocomposites

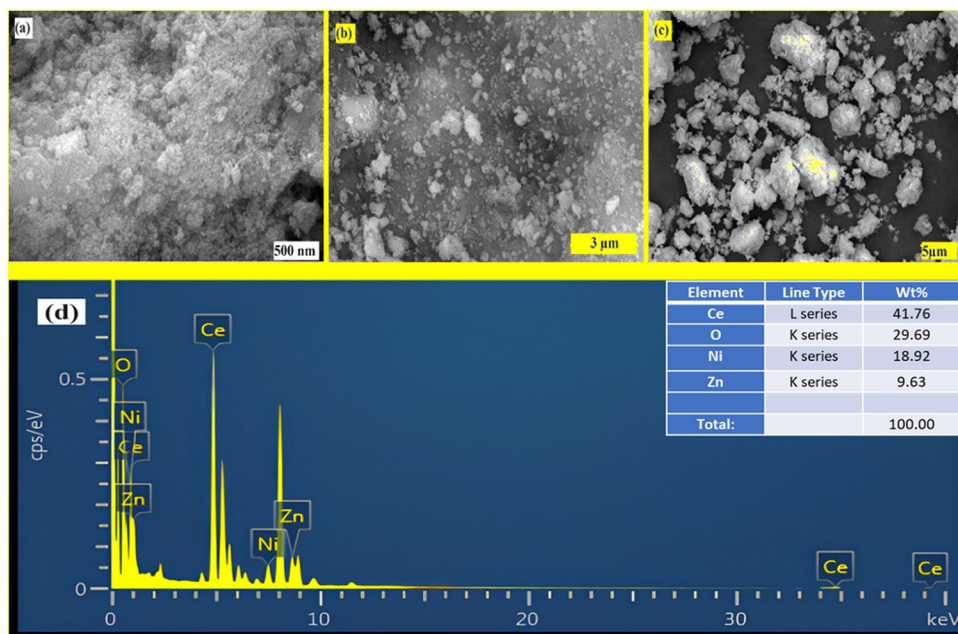
Nanocomposites	Peak at (before adsorption) (cm ⁻¹)	Functional groups (before adsorption)	Reference	Peak at (after adsorption) (cm ⁻¹)	Functional groups (after adsorption)	References
NZC 10:20:70 Fig. 3a–b	599.09	Zn-O	(Murali et al. 2017)	1109.18	C–O stretching vibrations	(Nurfani et al. 2020)
	1107.23	C–O stretching Vibrations	(Nurfani et al. 2020)	1484.23	vibration of the benzene ring	(Arya et al. 2023)
	1635.18	C=O stretching vibration	(Zhang et al. 2022)	3368.52	OH-Bond	(Shi et al. 2022)
	3305.48	strong absorption band of –O–H bond	(Shi et al. 2022)			
NZC 15:15:70 Fig. 3c–d	1114.89	symmetric C-O-C stretching	(Arya et al. 2023)	499.87	Zn-O	(Murali et al. 2017)
	3215.09	strong O-H stretching,	(Da Silva et al. 2019)	1206.23	Asymmetric C=O	(Balakrishnan et al. 2022)
				1150..37	Aromatic ring	(Al Lafi and Hay 2019)
				1484.24	vibration of the benzene ring	(Arya et al. 2023)
				3339.62	strong absorption band of –O–H bond	(Shi et al. 2022)

SEM analysis

The SEM images as shown in Fig. 4 of the Ni-Zn/CeO₂ nanomaterials (NZC 20:10:70) shows mixed distribution of nanoparticles, where some regions exhibit densely clustered aggregates while others showcase more dispersed individual nanoparticles.

The aggregations are predominantly comprised of CeO₂ nanoparticles, closely amalgamated with Zn and Ni nanoparticles (Manibalan et al. 2021). The minuscule size and consistent dispersion of the nanoparticles can be attributed to the stabilizing agent used during the synthesis process.

Fig. 4 SEM images of Ni-Zn/CeO₂ nanocomposites (NZC 20:10:70) **a** at 500 nm, **b** at 3 μm, **c** at 5 μm, and **d** EDAX analysis



TEM analysis

Transmission electron microscopy (TEM) analysis of as-synthesized Ni-Zn/CeO₂ nanomaterials (Fig. 5) indicates the average grain size for Ni-Zn/CeO₂ nanoparticles of 4.5 ± 1.0 nm. The high-resolution TEM image in Fig. 5b reveals lattice stripes of 0.528 nm and 1.08 nm of Ni-Zn/CeO₂ nanoparticles, corresponding to the (XYZ) and (XXZ) planes of CeO₂, respectively. The selected area electron diffraction (SAED) (Fig. 5c) demonstrates the diffraction rings assigned

to the orthorhombic phase of CeO₂, in agreement with the XRD analysis. The STEM and energy dispersive X-ray (EDX) elemental mapping (Fig. 5d) of this sample shows the presence and uniform distribution of Ce, Zn, Ni, and O.

BET analysis

The nitrogen adsorption/desorption isotherms were employed for the determination of the pore structure and surface area of all the synthesized Ni-Zn/CeO₂ nanomaterials.

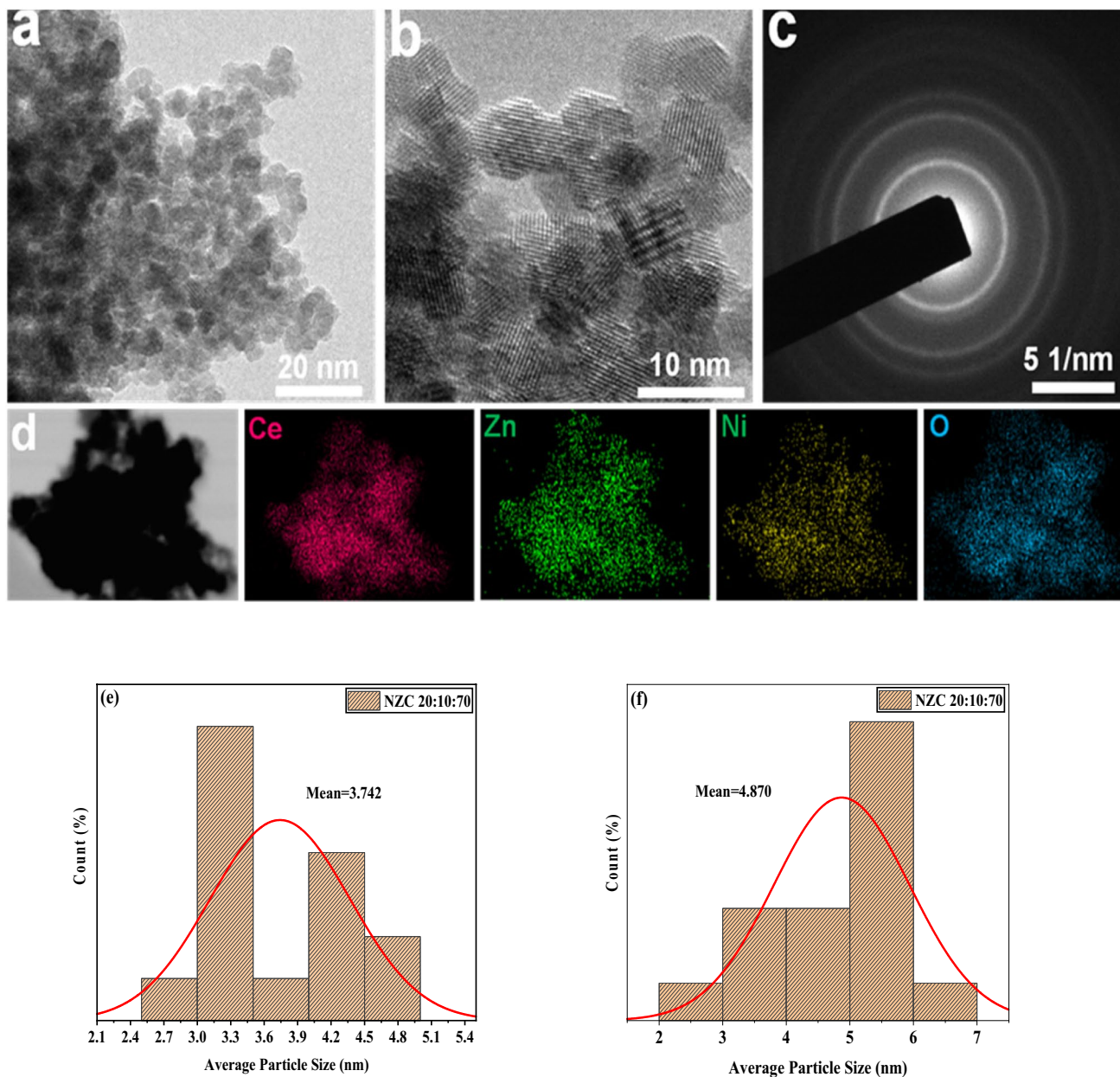


Fig. 5 TEM images at **a** NZC 20:10:70 (20 nm), **b** NZC 20:10:70 (10 nm), **c** SAED pattern of NZC 20:10:70, **d** EDS mapping pattern of NZC 20:10:70 nanocomposite and particles size distribution curve, **e** NZC 20:10:70 at 20 nm, **f** NZC 20:10:70 at 10 nm

As depicted in Fig. 6, the N₂ physisorption isotherm displayed Type IV behaviour as classified by the IUPAC standards indicating the presence of mesopores within the Ni-Zn/CeO₂ nanocomposite (Villaruel-Rocha et al. 2021) (Schlumberger and Thommes 2021). The textural characteristics of the synthesized nanomaterials are provided in Table 3. As it is evident, the mean pore diameter of all nanocomposites fell within the range typical of mesoporous materials. The results indicate that the surface area of the Ni-Zn/CeO₂ nanocomposites with compositions of 20:10:70 exhibited the highest surface area of 118.471 m²/g, respectively. The NZC 20:10:70 potentially promotes the formation of a more porous structure or enhances surface roughness, leading to increased surface area. Additionally, the larger pore diameter observed (6.448 nm) in NZC 20:10:70 suggests a more open pore structure, which contributes to its higher total pore volume (0.256 cc/g) (Liu et al. 2019).

The mesoporous structure of these nanomaterials is expected to play a critical role in boosting the adsorption of 4-chlorophenol molecules on their surface (*vide infra*). This is primarily due to the mesoporous structure's ability to facilitate the fast diffusion of 4-chlorophenol molecules through the adsorbent, thus improving the overall adsorption efficiency.

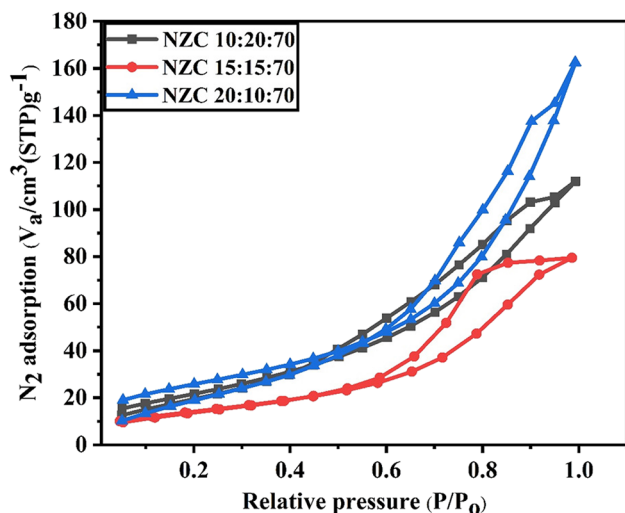


Fig. 6 BET nitrogen adsorption-desorption isotherms graphs of Ni-Zn/CeO₂ nanomaterials

Table 3 BET characteristics of Ni-Zn/CeO₂ nanocomposites

Nanomaterial	Surface area m ² /g	Total pore volume cc/g	Pore diameter (nm)
NZC 10:20:70	102.675	0.182	4.305 nm
NZC 15:15:70	62.252	0.193	3.813 nm
NZC 20:10:70	118.471	0.256	6.448 nm

TGA analysis

Thermogravimetric analysis (TGA) was used to explore the carbonation temperature, decomposition kinetics, and thermal stability of Ni-Zn/CeO₂ nanomaterials. As illustrated in Fig. 7a, the TGA findings for all compositions of Ni-Zn/CeO₂ nanocomposites unveiled a biphasic decomposition process during the pyrolysis. The first phase, occurring between 100 and 150 °C, involved dehydration, resulting in weight loss of 10% for 10:20:70, 8% for 15:15:70, and 5% for 20:10:70 compositions (Hsieh et al. 2018). In the subsequent stage, from 150 to 750 °C, the NZC 10:20:70 composition experienced a substantial 25% weight loss due to the pyrolytic decomposition of residues. Notably, the TGA curves for NZC 15:15:70 and NZC 20:10:70 showed a shift to higher temperatures (150–700 °C) with weight loss of around 10% and 14%, respectively. These trends are attributed to the decomposition of residues. TGA measurements were also undertaken for NZC 20:10:70 sample after the adsorption of 4-chlorophenol to evaluate the nanocomposite's stability. As shown in Fig. 7b, the nanocomposite remains stable even at elevated temperatures. The initial weight loss observed is due to the desorption of 4-chlorophenol that had been

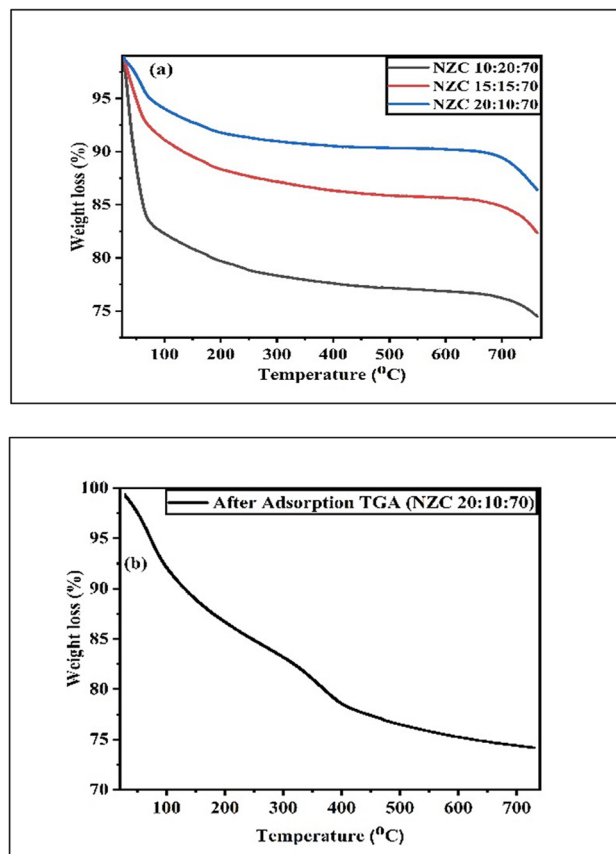


Fig. 7 TGA analysis: **a** TGA before adsorption and **b** TGA after adsorption (NZC 20:10:70)

Table 4 Analysis of variance (ANOVA) for 4-chlorophenol removal (%) by NZC 20:10:70 nanocomposite

Source	Sum of squares	d_f	Mean square	F -value	p Value	
Model ^a	14205.12	14	1014.65	60.29	<0.0001	significant
A-pH	756.92	1	756.92	44.97	<0.0001	
B-Contact time	3557.28	1	3557.28	211.35	<0.0001	
C-Adsorbent dose	94.47	1	94.47	5.61	0.0317	
D-Temperature	391.89	1	391.89	23.28	0.0002	
AB	155.55	1	155.55	9.24	0.0083	
AC	24.13	1	24.13	1.43	0.2497	
AD	172.44	1	172.44	10.25	0.0060	
BC	124.60	1	124.60	7.40	0.0158	
BD	40.27	1	40.27	2.39	0.1427	
CD	131.81	1	131.81	7.83	0.0135	
A ²	183.85	1	183.85	10.92	0.0048	
B ²	339.94	1	339.94	20.20	0.0004	
C ²	0.1705	1	0.1705	0.0101	0.9212	
D ²	176.15	1	176.15	10.47	0.0056	
Residual	252.46	15	16.83			
Lack of fit	118.79	9	13.20	0.5925	0.7696	Not significant
Pure error	133.67	6	22.28			
Cor total	14457.58	29				

^aThe model F -value of 60.29 indicates that the model is significant, with only a 0.01% probability that such a substantial that F -value could arise from random noise

adsorbed on the nanocomposite's surface. Once the entire 4-chlorophenol content is removed (typically occurring between 500 and 600 °C) (Tum and Kariuki 2020), the TGA curve stabilizes, indicating the nanocomposite's stability at higher temperatures.

Zeta potential analysis

The surface charge, characterized by zeta potential, significantly influences the adsorption of 4-chlorophenol onto Ni-Zn-CeO₂ nanocomposites. Under neutral conditions, the nanocomposite typically exhibits a slightly negative zeta potential value of -6 mV, while 4-chlorophenol remains predominantly neutral (Yang et al. 2017). During adsorption, interactions are primarily driven by weak forces such as hydrogen bonding and π - π or dipole-dipole interactions between the neutral molecules and the nanocomposite surface.

In acidic environments, the nanocomposite surface undergoes protonation, leading to a positively charged surface (Li et al. 2020). Despite 4-chlorophenol remaining neutral due to the presence of excess H⁺ ions, the positive surface charge creates a conducive environment for the molecules to approach and interact with the nanocomposite. In alkaline conditions where 4-chlorophenol exists predominantly as the phenolate ion (negatively charged), interactions between 4-chlorophenol and surfaces such as NZC nanocomposite would typically involve electrostatic repulsion rather than attraction (Zhang et al. 2019).

Analysis of variance and BBD model analysis

We employed the Box-Behnken Design under Response Surface Methodology (BBD-RSM) to investigate how different adsorption factors influenced the removal of 4-chlorophenol using the NZC 20:10:70 nanocomposite, which was identified as the most efficient among the three nanomaterials. The primary parameters examined included pH of the solution, temperature, adsorbent dosage, and contact time. A statistical analysis of the experimental results related to the removal of 4-chlorophenol by the NZC 20:10:70 nanocomposite was conducted using ANOVA, and the outcomes are tabulated in Table 4.

The ANOVA findings for NZC 20:10:70, particularly the F -values, indicate the quality of the models utilized, for 4-chlorophenol, in its removal. In this instance, the F -value for NZC 20:10:70 is 21.70, and the corresponding p ¹-value is less than 0.0001, implying a high degree of significance and data accuracy (Jawad et al. 2020). Generally, terms with p values above 0.05 are considered statistically insignificant in the context of 4-chlorophenol removal efficiency, and those with p values under 0.05 are considered statistically significant (Andrade 2019).

¹ The P value is like a measure of how likely it is that any differences we see between groups happened by random chance, assuming there is actually no real effect. It helps us figure out if our findings are reliable or just random [Dahiru 2011]. Model terms with p values less than 0.0500 are significant.

The R^2 (determination coefficient) for the removal of 4-chlorophenol is $ca \sim 0.9530$, indicating a close proximity between the experimental and calculated data.

As a result, the terms in the 4-chlorophenol removal model, including A, B, C, D, AB, AC, AD, BC, BD, CD, A^2 , B^2 , and C^2 , have been determined to be statistically significant. After performing the correlation analysis, second-order quadratic polynomial models involving the responses (4-chlorophenol removal) and the tested factors were established, as shown in Eq. 13 (analysed by Design Expert Software):

$$\begin{aligned} \text{Removal efficiency} : & + 60.9839 - 9.30995 A + 18.4774 B \\ & + 4.43128 C - 5.94134D - 3.58586AB \\ & + 3.80018AD + 4.47591BC + 3.18368CD \\ & - 11.7459 A^2 - 15.6631 B^2 + 14.2883 D \end{aligned} \quad (13)$$

Figure 8a illustrates the efficiency of the NZC 20:10:70 nanocomposite in removing 4-chlorophenol. As evident, the tightly clustered data points along a single line indicate the model's effectiveness and reliability of the ANOVA results (Kusuma et al. 2021). Figure 8b compares the predicted results with the actual results for the elimination of 4-chlorophenol. A strong alignment between the model's predictions and the actual observed outcomes indicates the reliability of the data used in the formulation of the model.

Synergistic effects of variables

The 3D response surface diagrams were plotted to assess the impact of various factors on the removal of 4-chlorophenol using NZC nanomaterials. Figure 9a and b depict the combined effects of adsorbent dosage (NZC 20:10:70) and pH on the rate of 4 chlorophenol removal, with temperature held constant at 10°C and a fixed contact time of 120 min.

From the results presented in Fig. 9a and b, it becomes clear that the adsorption efficiency of 4 chlorophenol by NZC 10:20:70 is significantly enhanced under acidic conditions at pH 3 and decreases as the pH becomes more basic, approaching pH 10. Meanwhile, as shown in Fig. 7b, the removal effectiveness of 4-chlorophenol is boosted by increasing the adsorbent dosage (from 10 to 50 mg) and contact time (10–20 min), while maintaining the pH at 3 and the temperature fixed at 10 °C. The maximum removal efficiency achieved by NZC 10:20:70 was 91.3%.

Figure 9c and d illustrate the adsorption of 4 chlorophenol by NZC 15:15:70 nanocomposites, and the same experimental conditions and parameters were followed as in the case of NZC 10:20:70, showing similar trends. However, this particular nanocomposite exhibits a lower adsorption capacity. Under optimal conditions of pH 3, a temperature of 10 °C, a contact duration of 120 min, and an adsorbent dosage of 50 mg, it achieves a maximum removal of 79.1%. These same experimental conditions

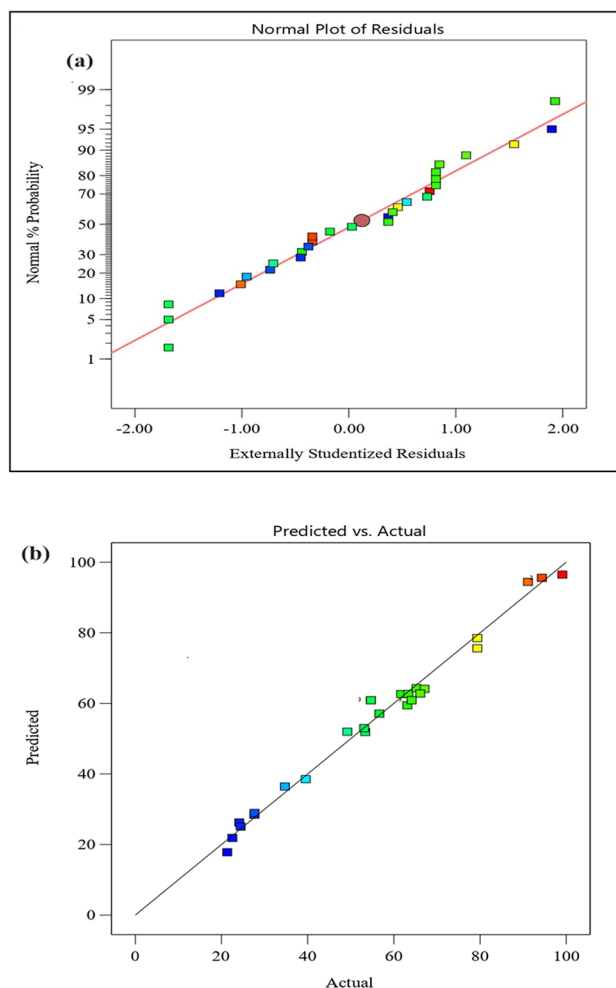


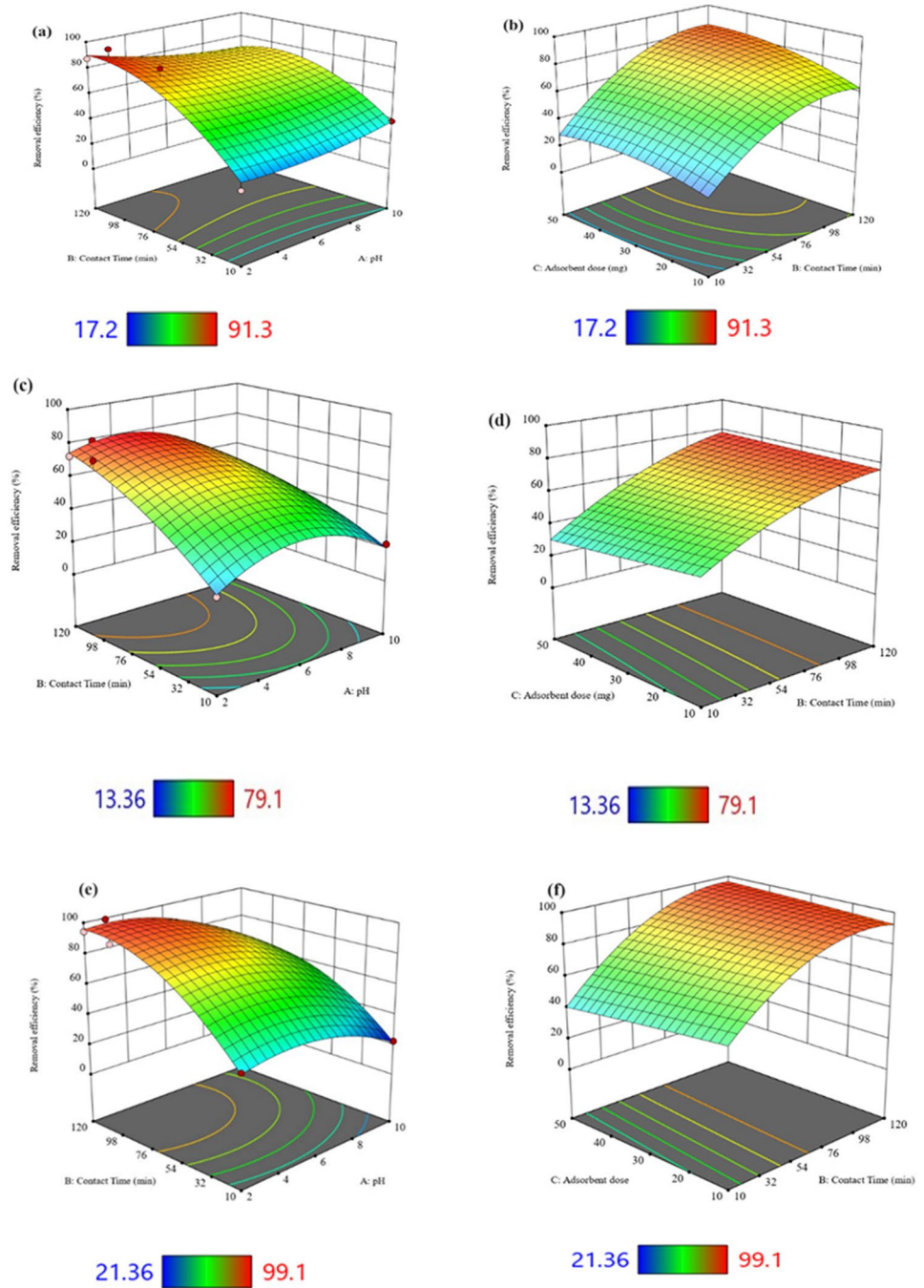
Fig. 8 **a** Normal probability plot of residuals for a NZC 20:10:70 nanocomposite. **b** Graphical representation depicting the correlation between predicted and actual values of 4 chlorophenol removal for NZC 20:10:70

and parameters were applied to NCC 20:10:70 nanocomposites (Fig. 9e and f) resulting in an impressive 99.1% removal of 4-chlorophenol in 120 min. In summary, these experiments allow us to deduce the optimal conditions and trends for 4-chlorophenol removal from NZC nanocomposites. Removal efficiency is higher under acidic pH conditions, while it decreases under alkaline pH. Both adsorbent dosage and contact time exhibit a similar pattern, with an increase in these parameters leading to enhanced removal of 4-chlorophenol. The temperature was kept at (lowest value) 10 °C in these responsive curve diagrams

Influence of concentration

The influence of concentration on removal efficiency was investigated by altering the concentration of 4-chlorophenol from 10 to 50 ppm while keeping a constant adsorbent

Fig. 9 A 3D response surface plots of significant interactions on 4-chlorophenol removal **a, b** from NZC 10:20:70, **c, d** from NZC 15:15:70, and **e, f** from NZC 20:10:70 (pH = 2–10, 4-CP concentration = 10–50 ppm, adsorbent dose = 10–50 mg, contact time = 10–120 min, T = 20 °C, volume of solution = 100 ml)



dosage of 50 mg at 20 °C and 120 min of contact time and pH 3.0. The results, as depicted in Fig. 10, clearly demonstrate a decline in removal efficiency with increasing 4-chlorophenol concentration. In the adsorption studies using different nanocomposites, the adsorption capacity (q_e) shows a consistent increase as the initial concentration of the solution rises from 10 ppm to 50 ppm. For NZC 10-20-70, q_e rises from 18.88 mg/g at 10 ppm to 92.47 mg/g at 50 ppm. Similarly, NZC 15-15-70 exhibits an increase in q_e from 17.82

mg/g at 10 ppm to 80.65 mg/g at 50 ppm, while NZC 20-10-70 demonstrates growth from 19.85 mg/g at 10 ppm to 96.33 mg/g at 50 ppm. For all three nanomaterials, achieving equilibrium at a higher concentration of 4-chlorophenol required a relatively longer period. The greater mass resistance that the adsorbate molecules experience when trying to penetrate through the deeper layers of the immobilized adsorbent is the cause of this extended equilibration time (Bahrudin et al. 2020).

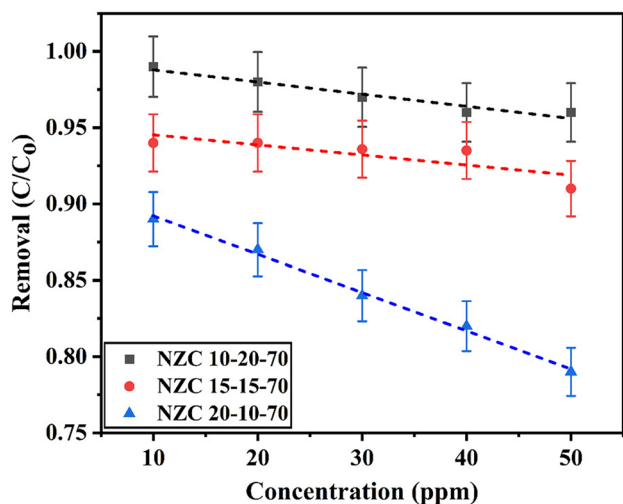


Fig. 10 Impact of concentration on removal efficiency of 4-chlorophenol by Ni-Zn/CeO₂ nanocomposites (pH=3, 4-CP concentration = 10–50 ppm, adsorbent dose = 0.05g, contact time = 120 min, T = 20 °C, volume of solution = 100 ml)

Influence of temperature

Temperature dependence of 4-chlorophenol removal by Ni-Zn/CeO₂ nanocomposites was examined within a temperature range of 10°C to 60°C (Fig. 11). The data reveal an inverse linear relationship between removal efficiency and temperature for all three nanocomposites. Low-temperature conditions favoured the removal of 4-chlorophenol, suggesting the involvement of weak adsorptive forces during the process. These forces are compromised by high temperatures lead to their disruption and finally causing a decline in the removal efficiency of 4-chlorophenol (Semwal et al. 2023).

Adsorption isotherm

The adsorption isotherm for NZC nanocomposites was studied by three models namely Langmuir, Freundlich, and Temkin models (Fig. 12a, b, and c respectively). The Freundlich model effectively described the adsorption phenomenon, as shown in Table 5. In comparison to Langmuir and Temkin isotherms, the R^2 values for Freundlich isotherms were higher for all three nanocomposites. The Freundlich isotherm model's R^2 value was in the range of 0.99 for all three nanocomposites indicating a strong fit. Additionally, the calculated heterogeneity factor (n) falls within the range of 1–3, suggesting that the reaction is favourable. If $1 < n < 10$, which confirms that the adsorption was favourable (Zhao et al. 2020). A combined analysis of the Langmuir (Fig. 12a) and Freundlich isotherm models (Fig. 12b) revealed that 4-chlorophenol adsorption onto NZC nanocomposites was a complex process comprising both chemical and physical adsorption, as well as monolayer and multilayer adsorption.

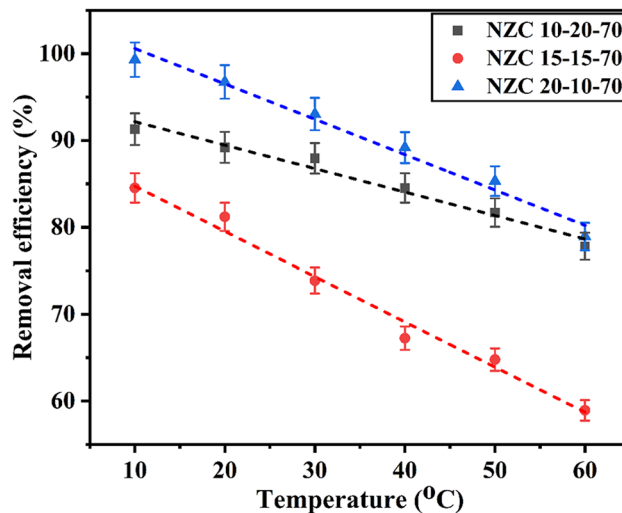


Fig. 11 Impact of temperature on removal efficiency of 4-chlorophenol by Ni-Zn/CeO₂ nanocomposites (pH = 3, 4-CP concentration = 50 ppm, adsorbent dose = 0.05g, contact time = 120 min, T = 10–60 °C, volume of solution = 100 ml)

The Temkin model's fitting results in this study were moderate (Fig. 12c). This finding suggests that electrostatic interaction is likely one of the mechanisms involved in the adsorption of 4-chlorophenol onto Ni-Zn/CeO₂ nanocomposites [Rajahmundry et al. 2021].

Thermodynamic parameters

Different thermodynamic parameters for the adsorption of 4-chlorophenols on the synthesized nanomaterials were determined and logically interpreted. These values are appended in Table 6.

The ΔG^0 values observed in the range of -0.4 to -1.7 kJ/mol (Fig. 13a) suggest a sorption process that begins as physisorption (physical adsorption). Physisorption is typically characterized by ΔG^0_{ads} values between 0 and -20 kJ/mol (Darla et al. 2023). The negativity of ΔG^0 supports the viability of 4-chlorophenol adsorption onto the synthesized Ni-Zn/CeO₂ nanocomposites, and the process of adsorption is spontaneous. A negative ΔS^0 value indicates the affinity of the Ni-Zn/CeO₂ nanocomposites for 4-chlorophenol and decreases in the randomness at the solid-solution interface (Kashipazha et al. 2023). The calculated values of ΔH^0 are negative, which confirms that the nature of the adsorption process is exothermic, aligning with the experimental data demonstrating a decrease in adsorption with increasing temperature (Jery et al. 2024). The higher the negative value ΔH^0 , the stronger the exothermic interaction between the 4-chlorophenol and the nanocomposite surface.

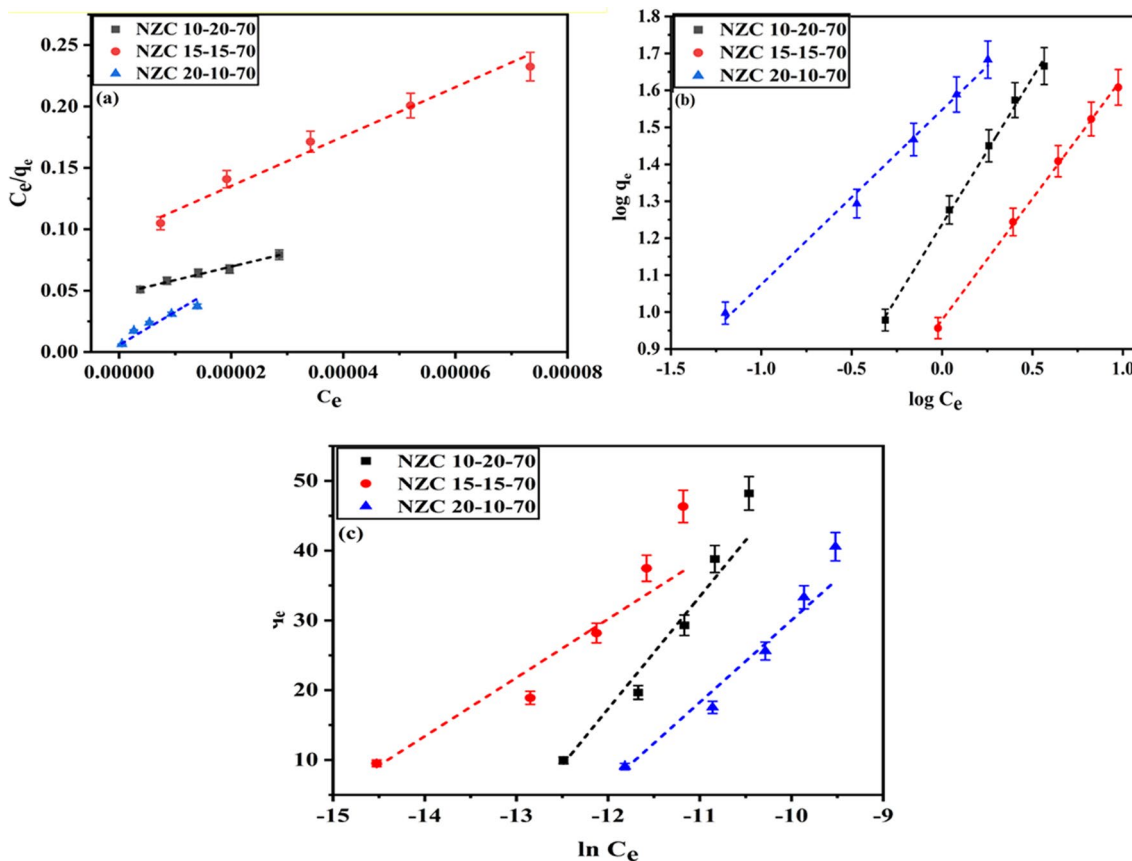


Fig. 12 Adsorption isotherm linear fitted plots of 4-CP by NZC nanocomposites **a** Langmuir, **b** Freundlich, and **c** Temkin isotherms (pH = 3 , 4-CP concentration = 10–50 ppm, adsorbent dose = 0.05 g, contact time = 120 min, T = 20 °C, volume of solution = 100 ml)

Table 5 Ni-Zn/CeO₂ nanocomposites' isotherm constants for the adsorption of 4-chlorophenol

Nanocomposites	Langmuir			Freundlich			Temkin	
	R^2_L	K_L	q_{max}	R^2_F	K_F	n	B	R^2
	(mg/g)			(mg/g)(Lmg ¹) ^{1/n}				
NZC 10:20:70	0.9864	0.329	118.2	0.9971	1.9*10 ⁵	1.25	16.103	0.9656
NZC 15:15:70	0.9775	0.277	68.27	0.9989	7.69*10 ⁵	1.52	08.399	0.9275
NZC 20:10:70	0.9383	0.014	59.1	0.9948	1.8*10 ⁶	2.11	11.763	0.9702

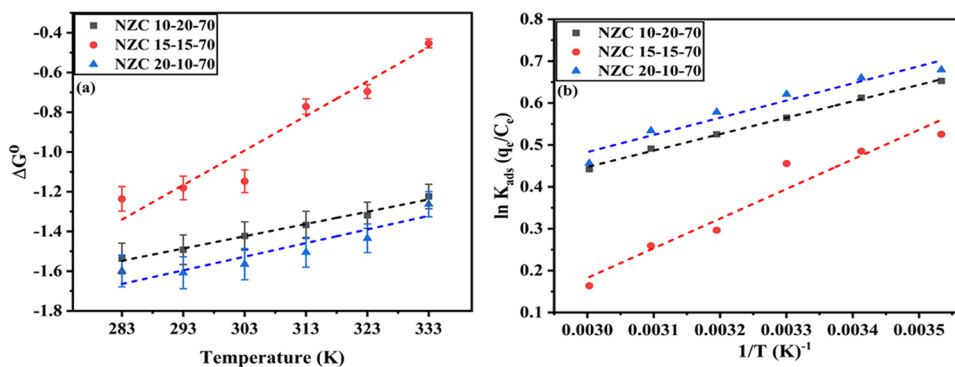
Table 6 Thermodynamic constants for adsorption of 4-chlorophenol on Ni-Zn/CeO₂ nanocomposites

Nanocomposite	ΔH^0 KJmol ⁻¹	ΔS^0 KJmol ⁻¹ K ⁻¹	R^2
NZC 10:20:70	- 3.26	- 6.0619	0.9957
NZC 15:15:70	- 5.88	- 16.1248	0.9276
NZC 20:10:70	- 3.40	- 6.2104	0.9307

Kinetic study

The kinetic models of pseudo-second-order (PSO) and pseudo-first-order (PFO) were applied in order to study the adsorption process of 4-chlorophenol (4-chlorophenol) onto Ni-Zn/CeO₂ nanocomposites. The higher R^2 values obtained for the PSO models (0.9996, 0.9980, and 0.9976) for the three nanocomposites, NZC 10:20:70, NZC 15:15:70, and NZC

Fig. 13 Thermodynamic study of adsorptive removal of 4-chlorophenol by Ni-Zn/CeO₂ nanocomposites kinetics studies: **a** ΔG° values at different temperature and **b** thermodynamic Van't Hoff plot ln K_{ads} vs 1/T (pH = 3, 4-CP concentration = 50 ppm, adsorbent dose = 0.05 g, contact time = 120 min, T = 10–60 °C (283–333 K), volume of solution = 100 ml)



20:10:70, respectively, indicate that the PSO model (Fig. 14b) suited the data obtained from experiment better than the PFO model (Fig. 14a) (Revellame et al. 2020; Simonin 2016). The enhanced efficacy of the PSO model implies that chemisorption, which involves the establishment of strong chemical interactions between 4-chlorophenol molecules and the nanocomposite surface, is the primary mechanism governing the adsorption process (Bagheri et al. 2022). Additionally, the proximity between the calculated adsorption capacity values ($q_{e\text{ calc}}$) from the PSO model and the experimental q_e values ($q_{e\text{ exp}}$) further supports the relevance of the PSO model in explaining the adsorption kinetics of 4-chlorophenol onto Ni-Zn/CeO₂ nanocomposites indicated in Table 7.

Desorption and reusability studies

The economic significance of adsorbent reusability must be overemphasized. In seeking this, the efficiency of adsorption was assessed over eight (8) consecutive cycles for the NZC

20:10:70 nanocomposite, with the adsorbent being isolated and subjected to multiple washes with NaOH and deionized water after each cycle (Tazik et al. 2023).

The reusability analysis was performed on NZC 20:10:70 nanocomposite as it gives the best removal efficiency among all the nanocomposites. As illustrated in Fig. 15, the findings indicated that the rate of adsorption was decreased by approximately 15% after eight regeneration cycles. This small decrease is significant because it shows that these nanocomposites can be reused many times without losing their effectiveness. For sustainability and cost-effective option, these nanocomposites should retain their adsorption performance over multiple uses.

Comparative analysis with existing literature

Table 8 summarises a comparative analysis of different nano-adsorbents, contact time for the removal, and the corresponding removal efficiencies for chlorophenol from aqueous solution.

Fig. 14 Non-linear fitted curve of **a** pseudo-first-order kinetics and **b** pseudo-second-order kinetics for adsorption of 4-chlorophenol on Ni-Zn/CeO₂ nanocomposites (pH = 3, 4-CP concentration = 50 ppm, adsorbent dose = 0.05 g, contact time = 20–120 min, T = 20 °C, volume of solution = 100 ml)

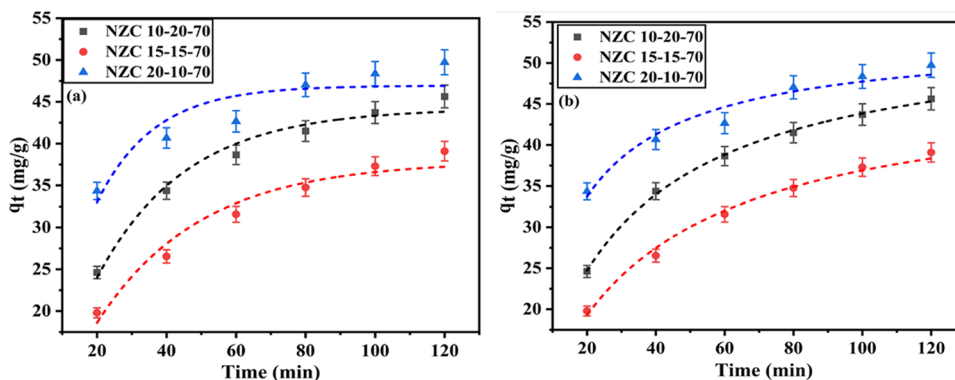


Table 7 The first and second-order kinetic models' parameters for the adsorption of 4-chlorophenol on the Ni-Zn/CeO₂ nanocomposite

Nanocomposite	First order				Second order			
	$q_e\text{ exp}$ mg g ⁻¹	$q_e\text{ calc}'$ mg g ⁻¹	k_1 min ⁻¹	R^2	$q_e\text{ exp}$ mg g ⁻¹	$q_e\text{ calc}'$ mg g ⁻¹	k_2 g mg ⁻¹ min ⁻¹	R^2
NZC 10:20:70	44.20	0.201	0.03	0.9828	45.63	54.37	7.65*10 ⁻⁴	0.9988
NZC 15:15:70	37.88	0.190	0.03	0.9607	39.09	47.81	7.06*10 ⁻⁴	0.9911
NZC 20:10:70	46.93	0.172	0.06	0.8345	49.72	55.24	1.62*10 ⁻³	0.9657

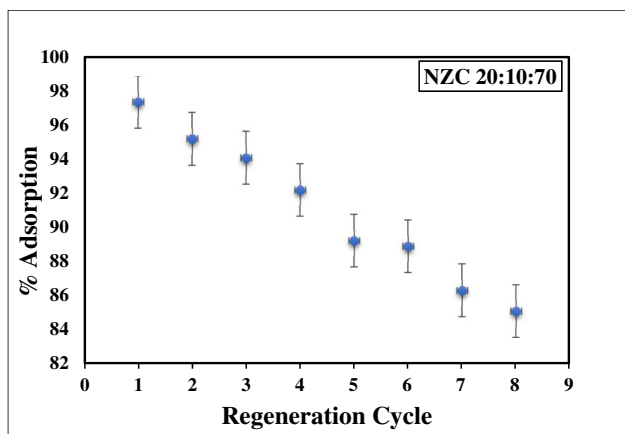


Fig. 15 Regeneration cycles of removal of 4-chlorophenol by using NZC 20:10:70 nanocomposite (pH = 3, 4-CP concentration = 50 ppm, adsorbent dose = 0.05 g, contact time = 120 min, T = 20 °C, volume of solution = 100 ml)

Adsorption mechanism

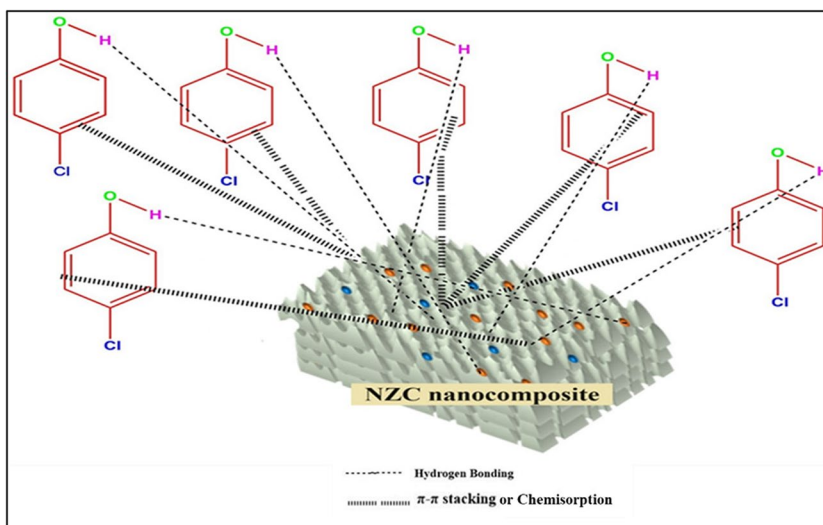
The adsorption of 4-chlorophenol onto Ni-Zn/CeO₂ nanocomposites is a multi-step process involving physical and chemical interactions. The FT-IR peak at 1515.31 cm⁻¹, representing C=C stretching of an aromatic group, proposes that the aromatic ring of 4-chlorophenol interacts with the nanocomposite surface via π-π stacking or hydrogen bonding. The close association of adsorbate molecules with the nanocomposite surface facilitates chemical bonds formation (chemisorption) between the surface and 4-chlorophenol molecules.

In addition to adsorption through chemical bond formation, the O-H bonds present on the surface of nanocomposites lead to hydrogen bonding interactions between 4-chlorophenol’s -OH groups. Overall, the proposed adsorption mechanism of 4-chlorophenol on Ni-Zn/CeO₂ nanocomposites involves physisorption, chemisorption, aromatic interactions, and hydrogen bonding as illustrated in Fig. 16.

Table 8 Comparative analysis of various adsorbents removal efficiency for the removal of 4-chlorophenol

S. No.	Adsorbent	Adsorption capacity (mg/g)	Contact time (min)	Removal efficiency (%)	References
1	Polymethylmethacrylate-bentonite	163.93	1440	~70	(Abu-Zurayk et al. 2023)
2	Activated carbon modified with amine groups	316.1	35	90%	(Tazik et al. 2023)
3	Carbon-based iron material	173.9	120	~100	(Wang et al. 2022)
4	Nitrogen doped carbon nanofiber	604.1	180	~70	(Gao et al. 2021)
5	Magnetic Fe ₃ O ₄ /activated carbon	128	60	>90	(Duan et al. 2020)
6	Magnetic biochar supported α-MnO ₂ nanorod	-	180	64	(Zhou et al. 2020)
7	Layered double hydroxides/single-walled carbon nanotubes	255.6	1440	99.20	(Zhang et al. 2019)
8	Ni-Zn/CeO ₂ nanocomposite	92.47	120	99.7%	This study

Fig. 16 Adsorption mechanism for removal of 4-chlorophenol by NZC nanocomposites



Conclusion

The Ni-Zn/CeO₂ nanocomposites were successfully synthesized using an aqueous co-precipitation method. It was demonstrated that the nanocomposites effectively remove 4-chlorophenol from aqueous solutions. The optimal conditions for this removal were identified as a solution pH of 3, an adsorbent dosage of 0.05 g/L, and a temperature of 10°C. XRD analysis confirmed the formation of two phases within the CeO₂ matrix. The pseudo-second-order kinetics and Freundlich isotherm were followed during the adsorption process. The adsorption of 4-chlorophenol is mainly facilitated by chemical forces, such as hydrogen bonding, π - π interactions. TEM analysis revealed that particle size ranges from 3 to 5 nm, and TGA analysis also confirmed that the nanocomposites can withstand high temperatures even post-adsorption process. The nanocomposite with the composition NZC 20:10:70 exhibited the highest removal capacity for 4-chlorophenol. This nanocomposite removed approximately 99.1% of 4-chlorophenol within an equilibrium time of 2 h. The nanocomposites exhibit excellent reusability, enabling their repeated use for removing phenolic pollutants.

Author contribution N.S.: conducted experiments, collected data, drafted the original manuscript

D.M.: conducted experiments, collected data

M.C.: data analysis, review

R.K.: data analysis

M.C.A.: conceptualisation, supervision, reviewing and editing of manuscript

Data availability The data will be made available on reasonable request.

Declarations

Consent to participate Not applicable.

Consent for publication Not applicable.

Competing interests The authors declare no competing interests.

References

- Abu-Zurayk RA, Hamadneh I, Al-Taei BJ, Al-Kayed MF, Al-Dujaili AH (2023) Adsorption of Pb(II) and Cr(III) ions and p-chlorophenol on polymethylmethacrylate-organobentonite Nanocomposite. *Polym Bull.* <https://doi.org/10.1007/s00289-023-05001-2>
- Adeyemi I, Sulaiman R, Almazroui M, Al-Hammadi A, Al Nashef I (2020) Removal of chlorophenols from aqueous media with hydrophobic deep eutectic solvents: experimental study and COSMO RS evaluation. *J Mol Liq* 311:113180. <https://doi.org/10.1016/j.molliq.2020.113180>
- Ajmi ASSA, Bosu S, Rajamohan N (2024) Biomass - metal oxide nano composite for the decontamination of phenol from polluted environment - parametric, kinetics and isotherm studies. *Environ Res* 240:117467. <https://doi.org/10.1016/j.envres.2023.117467>
- Al Lafi AG, Hay JN (2019) 2D-COS-FTIR analysis of high molecular weight poly (N-vinyl carbazole) undergoing phase separation on purification and thermal annealing. *J Mol Struct* 1175:152–162. <https://doi.org/10.1016/j.molstruc.2018.07.077>
- Al-Ghouthi MA, Al-Absi RS (2020) Mechanistic understanding of the adsorption and thermodynamic aspects of cationic methylene blue dye onto cellulosic olive stones biomass from wastewater. *Sci Rep* 10(1). <https://doi.org/10.1038/s41598-020-72996-3>
- Allaboun H, Al-Rub F a A (2016) Removal of 4-chlorophenol from contaminated water using activated carbon from dried date pits: equilibrium, kinetics, and thermodynamics analyses. *Materials* 9(4):251. <https://doi.org/10.3390/ma9040251>
- Al-Thabaiti SA, Khan Z, Malik MA (2019) Bimetallic Ag-Ni nanoparticles as an effective catalyst for hydrogen generation from hydrolysis of sodium borohydride. *Int J Hydrog Energy* 44(31):16452–16466. <https://doi.org/10.1016/j.ijhydene.2019.04.240>
- Andrade C (2019) The P value and statistical significance: misunderstandings, explanations, challenges, and alternatives. *Indian J Psychol Med* 41(3):210–215. https://doi.org/10.4103/ijpsym.ijpsym_193
- Arica TA, Balci FM, Balci S, Arica MY (2022) Highly porous Poly(o-phenylenediamine) loaded magnetic carboxymethyl cellulose hybrid beads for removal of two model textile dyes. *Fibers Polym* 23(10):2838–2854. <https://doi.org/10.1007/s12221-022-0221-4>
- Arya T, Bohra BS, Tewari C, Dhali S, Dikshit V, Rana S, Jung YC, Sahoo NG (2023) Influence of bio-resource-derived graphene oxide on the mechanical and thermal properties of poly(vinyl alcohol) nanocomposites. *Polym Compos.* <https://doi.org/10.1002/pc.27808>
- Ayawei N, Ebelegi AN, Wankasi D (2017) Modelling and interpretation of adsorption isotherms. *J Chem* 2017:1–11. <https://doi.org/10.1155/2017/3039817>
- Ayoob HW, Ridha AM, Jassim AA, Taieh NK, Homod RZ, Mohammed HI (2024) Enhanced adsorption of phenol using graphene oxide-bentonite nanocomposites: synthesis, characterisation, and optimisation. *J Mol Liq* 395:123833. <https://doi.org/10.1016/j.molliq.2023.123833>
- Azizi E, Abbasi F, Baghapour MA, Shirdareh MR, Shooshtarian MR (2021) 4-chlorophenol removal by air lift packed bed bioreactor and its modeling by kinetics and numerical model (artificial neural network). *Sci Rep* 11(1). <https://doi.org/10.1038/s41598-020-79968-7>
- Bagheri H, Pasha MA, Lakouraj MM, Hasantabar V, Mohseni M (2022) Highly efficient, bioactive, and bifunctional sorbent p–n–p visible light heterogeneous photocatalyst utilizing ultra-fine ZnS nanoparticles embedded in a polymeric nanocomposite. *RSC Adv* 12(25):15950–15972. <https://doi.org/10.1039/d2ra01810a>
- Bahadi SA, Drmash Q, Onaizi SA (2024) Adsorptive removal of organic pollutants from aqueous solutions using novel GO/bentonite/MgFeAl-LTH nanocomposite. *Environ Res* 248:118218. <https://doi.org/10.1016/j.envres.2024.118218>
- Bahrudin NN, Nawi MA, Jawad AH, Sabar S (2020) Adsorption characteristics and mechanistic study of immobilized chitosan-montmorillonite composite for methyl orange removal. *J Polym Environ* 28(7):1901–1913. <https://doi.org/10.1007/s10924-020-01734-7>
- Bai G, Wang J, Yang Z, Wang H, Wang Z, Yang S (2014) Preparation of a highly effective lubricating oil additive – ceria/graphene composite. *RSC Adv* 4(87):47096–47105. <https://doi.org/10.1039/c4ra09488c>

- Balakrishnan D, Usharani C, Pragathiswaran C, Rajivgandhi G, Maruthupandy M, Alharbi NS, Kadaikunnan S (2022) Synthesis and characterization of polyaniline doped with iron oxide nanocomposite using struvite crystal inhibition effect. *Chem Data Coll* 38:100843. <https://doi.org/10.1016/j.cdc.2022.100843>
- Basak M, Rahman ML, Ahmed MF, Biswas B, Sharmin N (2022) The use of X-ray diffraction peak profile analysis to determine the structural parameters of cobalt ferrite nanoparticles using Debye-Scherrer, Williamson-Hall, Halder-Wagner and Size-strain plot: Different precipitating agent approach. *J Alloys Compd* 895:162694. <https://doi.org/10.1016/j.jallcom.2021.162694>
- Bayramoglu G, Arica MY (2023) Biodegradation studies of phenol, diclofenac, and pentachlorophenol in a packed bed reactor loaded with immobilized white rot fungus *Leninus sajor-caju* biomass. *Water Air Soil Pollut* 234(10). <https://doi.org/10.1007/s11270-023-06634-9>
- Da Silva MN, De Matos Fonseca J, Feldhaus HK, Soares LS, Valencia GA, De Campos CEM, Di Luccio M, Monteiro AR (2019) Physical and morphological properties of hydroxypropyl methylcellulose films with curcumin polymorphs. *Food Hydrocoll* 97:105217. <https://doi.org/10.1016/j.foodhyd.2019.105217>
- Dahiru T (2011) P-Value, a true test of statistical significance? a cautionary note. *Ann Ibadan Postgrad Med* 6(1). <https://doi.org/10.4314/aipm.v6i1.64038>
- Darla UR, Lataye DH, Kumar A, Pandit B, Ubaidullah M (2023) Adsorption of phenol using adsorbent derived from *Saccharum officinarum* biomass: optimization, isotherms, kinetics, and thermodynamic study. *Sci Rep* 13(1). <https://doi.org/10.1038/s41598-023-42461-y>
- Doyo AN, Kumar R, Barakat MA (2023) Facile synthesis of the polyaniline@waste cellulosic nanocomposite for the efficient decontamination of copper(II) and phenol from wastewater. *Nanomaterials* 13(6):1014. <https://doi.org/10.3390/nano13061014>
- Duan Z, Zhang W, Lu M, Shao Z, Huang W, Li J, Li Y, Mo J, Li Y, Chen C (2020) Magnetic Fe₃O₄/activated carbon for combined adsorption and Fenton oxidation of 4-chlorophenol. *Carbon* 167:351–363. <https://doi.org/10.1016/j.carbon.2020.05.106>
- Emmett PH, Kummer JT (1943) Kinetics of ammonia synthesis. *Ind Eng Chem* 35(6):677–683. <https://doi.org/10.1021/ie50402a012>
- Freundlich H, Heller W (1939) The adsorption of cis- and transazobenzene. *J Am Chem Soc* 61(8):2228–2230. <https://doi.org/10.1021/ja01877a071>
- Gao Y, He D, Wu L, Wang Z, Yao Y, Huang ZH, Yang H, Wang MX (2021) Porous and ultrafine nitrogen-doped carbon nanofibers from bacterial cellulose with superior adsorption capacity for adsorption removal of low-concentration 4-chlorophenol. *Chem Eng J* 420:127411. <https://doi.org/10.1016/j.cej.2020.127411>
- Goel M, Chovelon JM, Ferronato C, Bayard R, Sreekrishnan T (2010) The remediation of wastewater containing 4-chlorophenol using integrated photocatalytic and biological treatment. *J Photochem Photobiol B Biol* 98(1):1–6. <https://doi.org/10.1016/j.jphotobiol.2009.09.006>
- Gómez M, Murcia MD, Ortega S, Barbosa DS, Vayá G, Hidalgo AM (2012) Removal of 4-chlorophenol in a continuous membrane bioreactor using different commercial peroxidases. *Desalin Water Treat* 37(1–3):97–107. <https://doi.org/10.1080/19443994.2012.661259>
- Guo Y, Zeng Z, Li Y, Huang Z, Yang J (2017) Catalytic oxidation of 4-chlorophenol on in-situ sulfur-doped activated carbon with sulfate radicals. *Sep Purif Technol* 179:257–264. <https://doi.org/10.1016/j.seppur.2017.02.006>
- Hamidon TS, Adnan R, Haafiz MKM, Hussin MH (2022) Cationic surfactant-modified cellulose nanocrystal/alginate hydrogel beads for enhanced adsorptive removal of 4-chlorophenol from wastewater. *J Polym Environ* 30(12):5024–5048. <https://doi.org/10.1007/s10924-022-02573-4>
- Ho Y, McKay G (1999) Pseudo-second order model for sorption processes. *Process Biochem* 34(5):451–465. [https://doi.org/10.1016/s0032-9592\(98\)00112-5](https://doi.org/10.1016/s0032-9592(98)00112-5)
- Hsieh W, Cheng W, Chen L, Lin S (2018) Non-isothermal dehydration kinetic study of aspartame hemihydrate using DSC, TGA and DSC-FTIR microspectroscopy. *Asian J Pharm Sci* 13(3):212–219. <https://doi.org/10.1016/j.ajps.2017.12.001>
- Jagaba AH, Lawal IM, Ghfar AA, Usman AK, Yaro NSA, Noor A, Abioye KJ, Birniwa AH (2023) Biochar-based geopolymer nanocomposite for COD and phenol removal from agro-industrial biorefinery wastewater: Kinetic modelling, microbial community, and optimization by response surface methodology. *Chemosphere* 339:139620. <https://doi.org/10.1016/j.chemosphere.2023.139620>
- Jawad AH, Abdulhameed AS, Malek NNA, ALOthman ZA (2020) Statistical optimization and modeling for color removal and COD reduction of reactive blue 19 dye by mesoporous chitosan-epichlorohydrin/kaolin clay composite. *Int J Biol Macromol* 164:4218–4230. <https://doi.org/10.1016/j.ijbiomac.2020.08.201>
- Jery AE, Alawamleh HSK, Sami M, Abbas HA, Sammen SS, Ahsan A, Imteaz MA, Shanableh A, Shafiq aman M, Osman H, Al-Ansari N (2024) Isotherms, kinetics and thermodynamic mechanism of methylene blue dye adsorption on synthesized activated carbon. *Sci Rep* 14(1). <https://doi.org/10.1038/s41598-023-50937-0>
- Kashipazha S, Tadayon F, Nematollahi F, Motiee F (2023) GO-Fe₃O₄-CeO₂-CTAB nanocomposite as a high-performance adsorbent for removal of phenol from aqueous solutions. *Int J Environ Anal Chem*:1–22. <https://doi.org/10.1080/03067319.2023.2182687>
- Ki SJ, Jeon KJ, Park YK, Jeong S, Lee H, Jung SC (2017) Improving removal of 4-chlorophenol using a TiO₂ photocatalytic system with microwave and ultraviolet radiation. *Catal Today* 293–294:15–22. <https://doi.org/10.1016/j.cattod.2016.12.023>
- Kumar N, Kumar B, Gupta H, Kumar A (2023) Development and evaluation of cellulose/graphene-oxide based composite for removing phenol from aqueous solutions. *Polymers* 15(3):572. <https://doi.org/10.3390/polym15030572>
- Kusuma HS, Amenaghawon AN, Darmokoesoemo H, Neolaka YA, Widyaningrum BA, Anyalewechi CL, Orukpe PI (2021) Evaluation of extract of *Ipomoea batatas* leaves as a green coagulant–floculant for turbid water treatment: parametric modelling and optimization using response surface methodology and artificial neural networks. *Environ Technol Innov* 24:102005. <https://doi.org/10.1016/j.eti.2021.102005>
- Lagergren S (1898) Zur theorie der sogenannten adsorption geloster stoffe. *Kungl Sven Vetensk Handl* 24(4):1–39. <https://sid.ir/paper/572485/en>
- Lan D, Zhu H, Zhang J, Li S, Chen Q, Wang C, Wu T, Xu M (2022) Adsorptive removal of organic dyes via porous materials for wastewater treatment in recent decades: a review on species, mechanisms and perspectives. *Chemosphere* 293:133464. <https://doi.org/10.1016/j.chemosphere.2021.133464>
- Langmuir I (1918) The adsorption of gases on plane surfaces of glass, mica and platinum. *J Am Chem Soc* 40(9):1361–1403. <https://doi.org/10.1021/ja02242a004>
- Li Z, Shan X, Chen Z, Gao N, Zeng W, Zeng X, Mei L (2020) Applications of surface modification technologies in nanomedicine for deep tumor penetration. *Adv Sci* 8(1). <https://doi.org/10.1002/advs.202002589>
- Liu Y, Rath B, Tingart M, Eschweiler J (2019) Role of implants surface modification in osseointegration: a systematic review. *J Biomed Mater Res A* 108(3):470–484. <https://doi.org/10.1002/jbm.a.36829>
- Lu B, Wang L, Zheng X, Hu Z, Pan Z (2019) Co-metabolic biodegradation of 4-chlorophenol by photosynthetic bacteria. *Environ Technol* 42(15):2361–2371. <https://doi.org/10.1080/09593330.2019.1701567>

- Manibalan G, Kumar MR, Murugadoss G, Yesuraj J, Kumar RM, Jayavel R (2021) Novel chemical route for synthesis of CeO₂-Zn nanocomposite towards high electrochemical supercapacitor application. *J Mater Sci Mater Electron* 32(7):8746–8755. <https://doi.org/10.1007/s10854-021-05546-w>
- Melchor-Lagar V, Ramos-Ramírez E, Morales-Pérez AA, Rangel-Vázquez I, Del Angel G (2020) Photocatalytic removal of 4-chlorophenol present in water using ZrO₂/LDH under UV light source. *J Photochem Photobiol A Chem* 389:112251. <https://doi.org/10.1016/j.jphotochem.2019.112251>
- Mishra SR, Roy P, Gadore V, Ahmaruzzaman M (2023) A combined experimental and modeling approach to elucidate the adsorption mechanism for sustainable water treatment via In₂S₃-anchored chitosan. *Sci Rep* 13(1). <https://doi.org/10.1038/s41598-023-45506-4>
- Murali M, Mahendra C, Nagabhushan, Rajashekar N, Sudarshana M, Raveesha K, Amruthesh K (2017) Antibacterial and antioxidant properties of biosynthesized zinc oxide nanoparticles from *Ceropegia candelabrum* L. – an endemic species. *Spectrochim Acta A Mol Biomol Spectrosc* 179:104–109. <https://doi.org/10.1016/j.saa.2017.02.027>
- Nurfani E, Kadja GTM, Purbayanto MAK, Darma Y (2020) The role of substrate temperature on defects, electronic transitions, and dark current behavior of Zn films fabricated by spray technique. *Mater Chem Phys* 239:122065. <https://doi.org/10.1016/j.matchemphys.2019.12>
- Pancholi MJ, Khristi A, Athira MK, Bagchi D (2022) Comparative analysis of lignocellulose agricultural waste and pre-treatment conditions with FTIR and machine learning modeling. *BioEnergy Res* 16(1):123–137. <https://doi.org/10.1007/s12155-022-10444-y>
- Patel N, Shahane S, Bhunia B, Mishra U, Chaudhary VK, Srivastav AL (2022) Biodegradation of 4-chlorophenol in batch and continuous packed bed reactor by isolated *Bacillus subtilis*. *J Environ Manag* 301:113851. <https://doi.org/10.1016/j.jenvman.2021.113851>
- Qasim I, Mumtaz M, Nadeem K, Abbas S (2016) Zinc nanoparticles at intercrystallite sites of (Cu_{0.5}Tl_{0.5})Ba₂Ca₃Cu₄O₁₂- δ Superconductor. *J Nanomater* 2016:1–6. <https://doi.org/10.1155/2016/9781790>
- Rahman N, Ahmad I (2023) Insights into the statistical physics modeling and fractal like kinetic approach for the adsorption of As(III) on coordination polymer gel based on zirconium(IV) and 2-thio-barbituric acid. *J Hazard Mater* 457:131783. <https://doi.org/10.1016/j.jhazmat.2023.131783>
- Rajahmundry GK, Garlapati C, Kumar PS, Alwi RS, Vo D-VN (2021) Statistical analysis of adsorption isotherm models and its appropriate selection. *Chemosphere* 276:130176. <https://doi.org/10.1016/j.chemosphere.2021.13>
- Ramasamy V, Mohana V, Rajendran V (2018) Characterization of Ca doped CeO₂ quantum dots and their applications in photocatalytic degradation. *OpenNano* 3:38–47. <https://doi.org/10.1016/j.onano.2018.04.002>
- Revellame E, Fortela DL, Sharp W, Hernández R, Zappi ME (2020) Adsorption kinetic modeling using pseudo-first order and pseudo-second order rate laws: a review. *Clean Eng Technol* 1:100032. <https://doi.org/10.1016/j.clet.2020.100032>
- Rodrigues A, Meera V, Vinod P (2024) Removal of phenol from aqueous solution using montmorillonite-Fe₃O₄-humic acid (MFH) nanocomposite. *IOP Conf Ser Earth Environ Sci* 1326(1):012074. <https://doi.org/10.1088/1755-1315/1326/1/012074>
- Saravanan R, Karthikeyan N, Gupta VK, Thirumal E, Thangadurai P, Narayanan V, Stephen A (2013) ZnO/Ag nanocomposite: an efficient catalyst for degradation studies of textile effluents under visible light. *Mater Sci Eng C* 33(4):2235–2244. <https://doi.org/10.1016/j.msec.2013.01.046>
- Schlumberger C, Thommes M (2021) Characterization of hierarchically ordered porous materials by physisorption and Mercury Porosimetry—a tutorial review. *Adv Mater Interfaces* 8(4). <https://doi.org/10.1002/admi.202002181>
- Semwal N, Mahar D, Chatti M, Dandapat A, Arya MC (2023) Adsorptive removal of Congo Red dye from its aqueous solution by Ag–Cu–CeO₂ nanocomposites: adsorption kinetics, isotherms, and thermodynamics. *Heliyon* 9(11):e22027. <https://doi.org/10.1016/j.heliyon.2023.e22027>
- Shi F, Zhuang X, Cui C, Zhang S (2022) Synthesis, characterization and scale inhibition performance evaluation of novel dendrimers with the initiator core of pentaerythritol derivative. *Desalination* 528:115632. <https://doi.org/10.1016/j.desal.2022.115632>
- Simonin J (2016) On the comparison of pseudo-first order and pseudo-second order rate laws in the modeling of adsorption kinetics. *Chem Eng J* 300:254–263. <https://doi.org/10.1016/j.cej.2016.04.079>
- Tazik M, Dehghani MH, Yaghmaeian K, Nazmara S, Salari M, Mahvi AH, Nasserri S, Soleimani H, Karri RR (2023) 4-Chlorophenol adsorption from water solutions by activated carbon functionalized with amine groups: response surface method and artificial neural networks. *Sci Rep* 13(1). <https://doi.org/10.1038/s41598-023-35117-4>
- Tran HN, Lima EC, Juang R, Bollinger J, Chao H (2021) Thermodynamic parameters of liquid–phase adsorption process calculated from different equilibrium constants related to adsorption isotherms: a comparison study. *J Environ Chem Eng* 9(6):106674. <https://doi.org/10.1016/j.jece.2021.106674>
- Tum P, Kariuki DK (2020) Photocatalytic degradation of 4-chlorophenol by titanium dioxide: role of annealing temperature and morphology. *J Appl Sci Environ Manag* 24(1):5. <https://doi.org/10.4314/jasem.v24i1.1>
- Varsha M, Senthil Kumar P, Senthil Rathi B (2022) A review on recent trends in the removal of emerging contaminants from aquatic environment using low-cost adsorbents. *Chemosphere* 287:132270. <https://doi.org/10.1016/j.chemosphere.2021.132270>
- Villaluz FJA, de Luna MDG, Colades JI, Garcia-Segura S, Lu MC (2019) Removal of 4-chlorophenol by visible-light photocatalysis using ammonium iron(II) sulfate-doped nano-titania. *Process Saf Environ Prot* 125:121–128. <https://doi.org/10.1016/j.psep.2019.03.001>
- Villarroel-Rocha J, Barrera D, Arroyo-Gómez J, Sapag K (2021) Insights of adsorption isotherms with different gases at 77 K and their use to assess the BET area of Nanoporous silica materials. *Adsorption* 27(7):1081–1093. <https://doi.org/10.1007/s10450-021-00339-3>
- Wang X, Yang L, Zhang J, Wang C, Li Q (2014) Preparation and characterization of chitosan–poly(vinyl alcohol)/bentonite nanocomposites for adsorption of Hg(II) ions. *Chem Eng J* 251:404–412. <https://doi.org/10.1016/j.cej.2014.04.089>
- Wang Y, Wang H, Wang L, Cai B, Chen H (2022) Removal of high-concentration 4 - Chlorophenol (4-chlorophenol) in wastewater using carbon-based heterogeneous catalytic oxidation: performance and mechanism. *J Clean Prod* 346:131176. <https://doi.org/10.1016/j.jclepro.2022.131176>
- Yadav S, Kumar S, Haritash AK (2023) A comprehensive review of chlorophenols: fate, toxicology and its treatment. *J Environ Manag* 342:118254. <https://doi.org/10.1016/j.jenvman.2023.118254>
- Yang F, Wu W, Chen S, Gan W (2017) The ionic strength dependent zeta potential at the surface of hexadecane droplets in water and the corresponding interfacial adsorption of surfactants. *Soft Matter* 13(3):638–646. <https://doi.org/10.1039/c6sm02174c>
- Zhang M, Ding R, Hu F (2022) Comparison on FTIR spectrum and thermal analysis for four types of Rehmannia Glutinosa and their extracts. <https://doi.org/10.21203/rs.3.rs-1319441>
- Zhang Z, Sun D, Li G, Zhang B, Zhang B, Qiu S, Li Y, Wu T (2019) Calcined products of Mg–Al layered double hydroxides/single-walled carbon nanotubes nanocomposites for expeditious removal

- of phenol and 4-chlorophenol from aqueous solutions. *Colloids Surf A Physicochem Eng Asp* 565:143–153. <https://doi.org/10.1016/j.colsurfa.2019.01.001>
- Zhao J, Wang C, Wang S, Zhou Y (2020) Experimental and DFT study of selective adsorption mechanisms of Pb(II) by UiO-66-NH₂ modified with 1,8-dihydroxyanthraquinone. *J Ind Eng Chem* 83:111–122. <https://doi.org/10.1016/j.jiec.2019.11.019>
- Zhao Z, Zhang J, Yao J, You S (2022) Electrochemical removal of 4-chlorophenol in water using a porous Magnéli-phase (Ti₄O₇) electrode. *Environ Res* 210:113004. <https://doi.org/10.1016/j.envres.2022.113004>
- Zhou H, Zhu X, Chen B (2020) Magnetic biochar supported α -MnO₂ nanorod for adsorption enhanced degradation of 4-chlorophenol via activation of peroxydisulfate. *Sci Total Environ* 724:138278. <https://doi.org/10.1016/j.scitotenv.2020.138278>

Publisher's Note Springer Nature remains neutral with regard to jurisdictional claims in published maps and institutional affiliations.

Springer Nature or its licensor (e.g. a society or other partner) holds exclusive rights to this article under a publishing agreement with the author(s) or other rightsholder(s); author self-archiving of the accepted manuscript version of this article is solely governed by the terms of such publishing agreement and applicable law.